Evaluation of tectonic structure of Gelibolu (Turkey) using steerable filters[1]

Osman N. Ucan[1], A. Muhittin Albora[2], Atilla Ozmen[3]

[1]Istanbul University, Engineering Faculty, Electrical-Electronics Eng. Dept.,34850, Avcilar, Istanbul, Turkey
[2] Istanbul University, Engineering Faculty, Geophysics Eng. Dept., 34850, Avcilar, Istanbul, Turkey
[3]Kadir Has University, Engineering Faculty, Electronics Eng. Dept., Eminonu, Istanbul, Turkey
E-mail: uosman@istanbul.edu.tr; muhittin@istanbul.edu.tr

Abstract: Steerable filters are oriented filters generally used in vision and image processing tasks, such as texture analysis, edge detection, image data compression, motion analysis, and image enhancement. Steerable filters with oriented property can be examined as a function of both orientation and phase. In the case of correct filter set and interpolation rules, it is possible to determine the response of a filter of arbitrary orientation without applying that filter directly.

In this paper, we have first applied steerable filters to synthetic examples and after satisfactory results are obtained; we have evaluated the tectonic setting of the Gelibolu Peninsula in the western region of Turkey using potential fields. The gravity and magnetic anomaly maps of Gelibolu used which was obtained from Turkish Petroleum Research Institute (TPAO). A parallel fault branch on the North-West of Anafartalar fault was detected. Also other tectonic structures of area were modelled. The results are confirmed by the TPAO seismic data. Further it is shown that steerable filters can be considered as a compromising approach in the evaluation of geophysical data. In particular, they can be used to delineate the strike of faults and to locate roughly ruins of foundation walls.

Keywords: Steerable filters, gravity and magnetic anomaly, Gelibolu region.

Introduction

In potential fields surveys, the observed data comprise the sum of the effects produced by all underground sources. The targets are often small-scale structures buried at shallow depths. The response of these targets is superimposed in a regional field which arises from underground sources that are usually larger in size or buried deeper. Correct estimation and removal of the regional field from the initial field observation, yields the residual field produced by the target sources. One of the main aims in geophysics is to detect the edges of underground structures. These edges are generally estimated by evaluation of the points where the curvature changes. In recent years, n contemporary image processing techniques such as wavelet analysis (Fedi and Quata, 1998), Markov Random Field (Ucan et al., 2001a), Cellular Neural Network (Albora et al., 2001a, 2001b) have been applied to geophysics for edge detection, enhancement and separation of potential fields anomalies.

Wavelet transforms are relatively a new way of decomposing a signal into its components, which carry information about the frequency (either directly or along scale information) content of the signal. Wavelet functions can be grouped in two main types: discrete and continuous. Haar function is an important discrete wavelet form and Mexican Hat, Morlet, Meyer, Battle-Lemarie are the main continuous wavelet functions (Rao and Bopardikar, 1998).

The stochastic models depending on Markov Random Field (MRF) approach in 2-

D data analysis have led to the development of many practical algorithms (Geman and Geman, 1984; Derin and Elliot, 1987) that would not have been realised with *ad-hoc* processing.   The objective of MRF modelling is to capture the intrinsic character of data in a few parameters so as to understand the nature of the phenomenon generating the data.

Chua and Yang (1988) introduced Cellular Neural Network (CNN) for the evaluation of real time 2-D images. CNN is composed of non-linear analogy circuits, which evaluates the neighbouring pixels and locality of their connections in real time. Because it is being composed of analogue elements, CNN is a high-speed real time processing system. CNN is an algorithm-based optimisation of real data under many constraints.   Chua and Thiran (1991) proposed a simple learning algorithm similar to linear 2-D filters. Zou and Nossek (1991) have analysed this problem as an inequality set of weight coefficients related with input-output parameters. Bilgili et al., (2002) have studied the genetic algorithm in training.

Blakely and Simpson (1986) have studied the detection of the edges of buried objects using boundary analysis in potential field data. Fedi and Floria (2001), used Enhanced Horizontal Derivative (EHD) method for the estimation of horizontal location of   potential fields source boundaries. Ucan et al., (2001b) have applied wavelet approach to interpret the gravity and magnetic data of Saros Bay in Turkey.

As one of the contemporary approaches, steerable filters have the directional property and the have been applied successfully among others, to biomedical data, hand-written character recognition, fault analysis, border detection. Steerable filters were first defined by Freeman and Adelson (1991), and then studied by many scientists such as Laine and Chang (1995), Ozmen (2001).   There are various approaches in the application of these filters.   One approach is to apply many versions of the same steerable filter, each different from the others by some small rotation in angle. A more efficient approach is to apply a few filters corresponding to a few angles and interpolate between the results.

In this paper, we use steerable filters in edge detection of the faults and their directions using gravity and magnetic anomaly maps as input. We demonstrate the procedure on both synthetic and real data. We apply steerable filter for Gelibolu region of Turkey. We model the region regarding steerable filter outputs.   The results are compared to results interred from seismic data and geological studies. The comparison shows that a good agreement exists between various approaches.

Steerable filters

In geophysics, one of the main problems is to delineate the edges of the buried objects. The detection of borders of subsurface bodies can be investigated by using either derivative based classical approaches or contemporary image processing algorithms such as steerable filters.   These filters with directional properties can be used in detection of the borders faults or other geometric structures such as walls of historical sites. Steerable filters were first defined by Freeman and Adelson (1991), and then studied by many scientists such as Laine and Chang (1995), Ozmen (2001). In steerable filters, impulse function $h^{\theta_a}(x,y)$ of any arbitrary angle θ_a, can be expressed as a combination of basis functions $h^{\theta_i}(x,y)$, $i = 1,..,M$ as (Freeman and Adelson, 1991),

$$h^{\theta_a}(x,y) = \sum_{i=1}^{M} k_i(\theta_a) h^{\theta_i}(x,y) \qquad (1)$$

where $k_i(\theta_a)$, $1 \le i \le M$, are the filter coefficients (Figure 1). Here, it is necessary to define which functions $h(x,y)$ can satisfy Equation 1 and what are the interpolation functions $k_i(\theta)$. Let *h* be any function which can be expanded in a Fourier series in polar angle θ as,
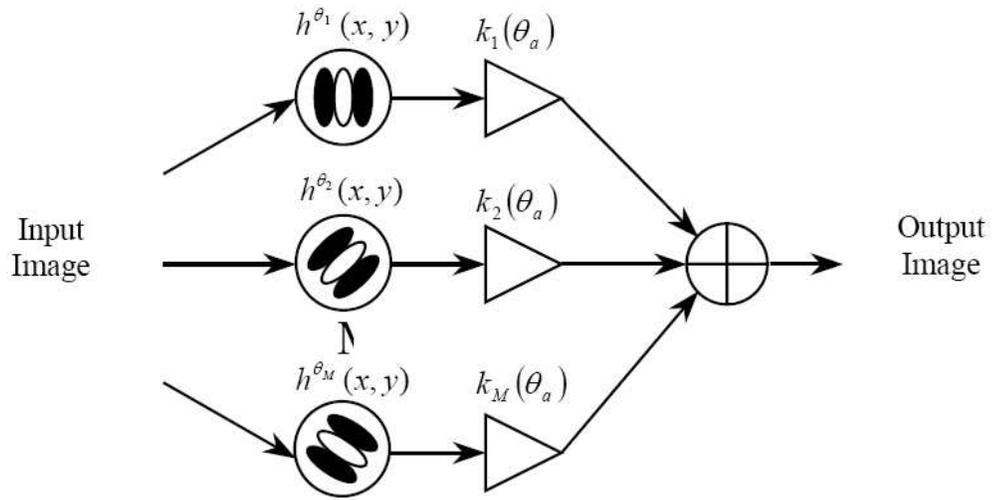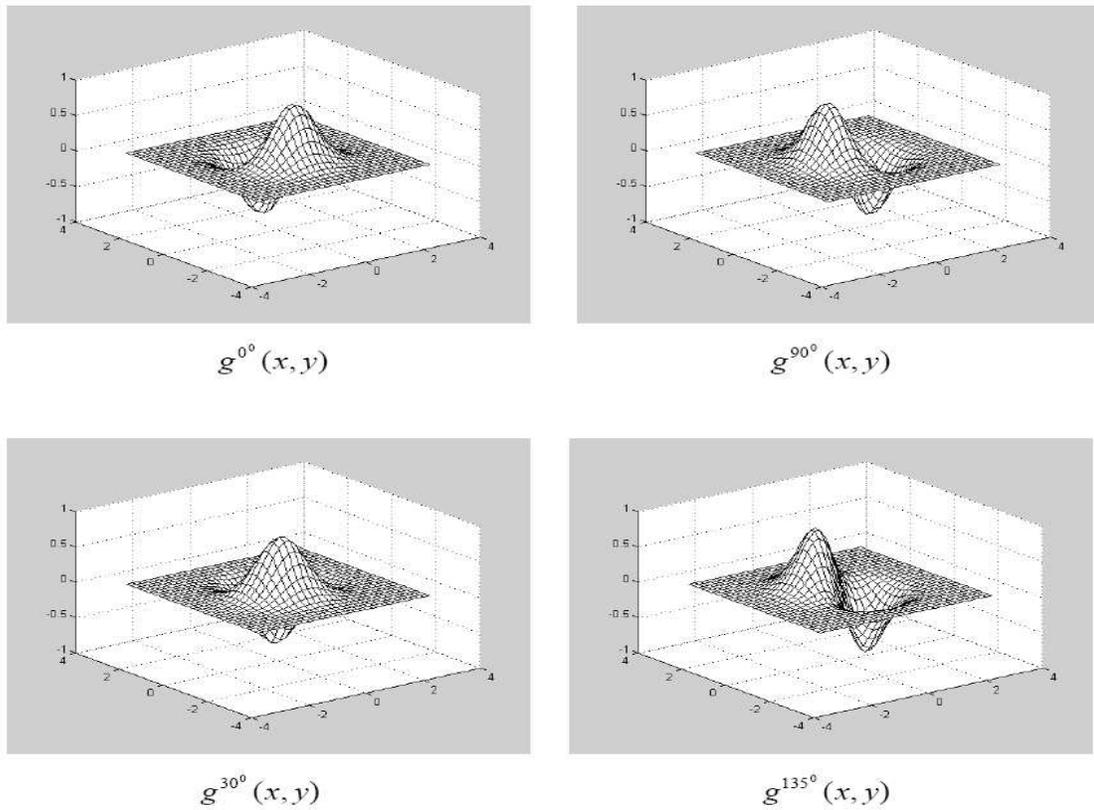
Fig 1. Block diagram of steerable filter.

$g^{0^0}(x,y)$

$g^{90^0}(x,y)$

$g^{30^0}(x,y)$

$g^{135^0}(x,y)$

Fig 2. Steerable filter outputs for 0 and 90 degrees
and for their linear combinations 45 and 135 degrees.
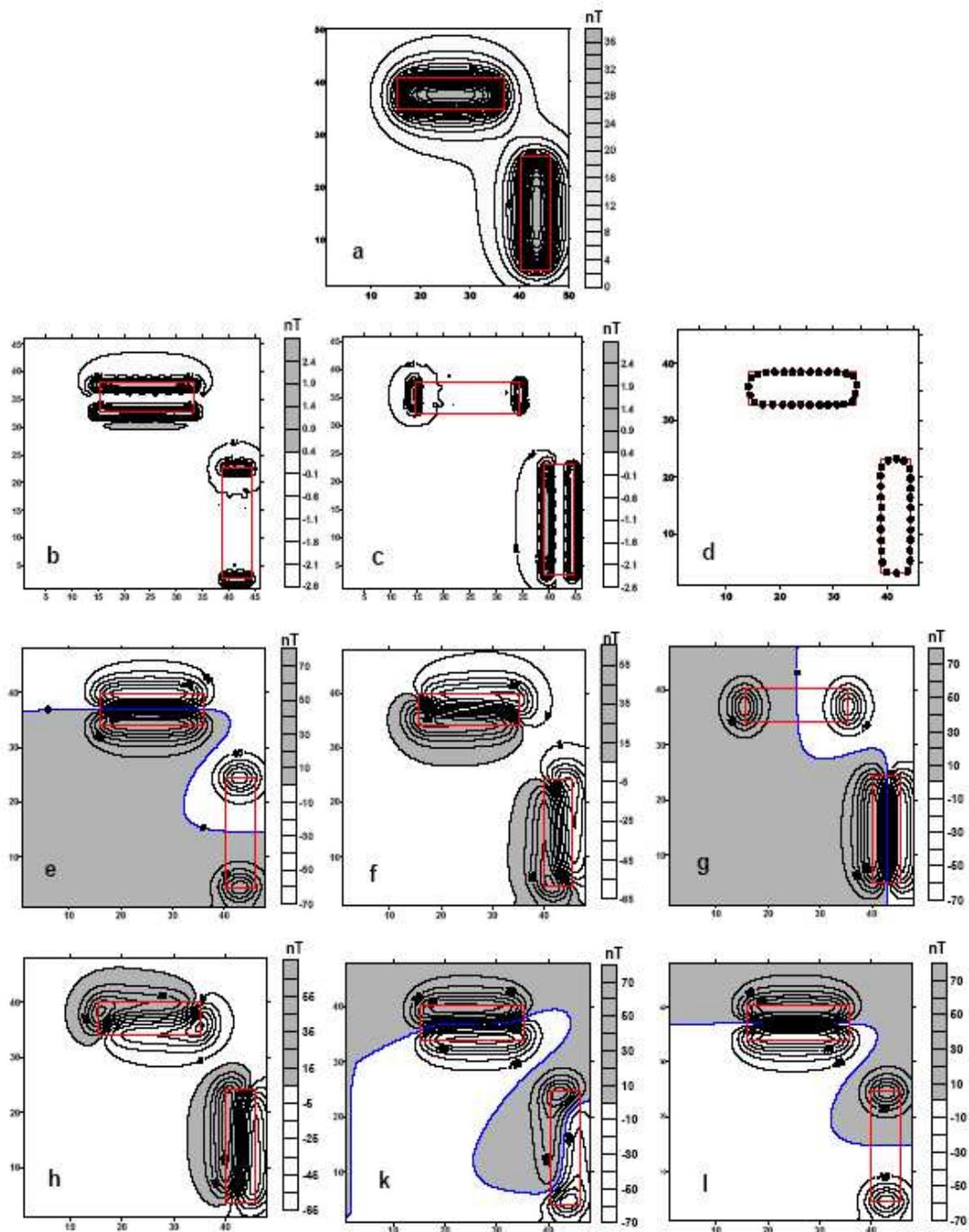
Osman n. Ucan

Fig 3. Two perpendicular vertical prism model (in dashed lines) with properties in Table I **a.** Total magnetic anomaly map (interval contour is 2 nT) **b.** Shift and Difference Horizontal filter output (interval contour is 0.5 nT) **c.** Shift and Difference Vertical filter output (interval contour is 0.5 nT) **d.** Boundary analysis output. **e.** Steerable filter output for the input data of total magnetic anomaly map in Figure 3a with 0^0 arbitrary angle **f.** with 40^0 **g.** with 90^0 **h.** with 120^0 **k.** with 160^0 **l.** with 180^0 (contour interval is 10 nT).

$$h(r,\theta) = \sum_{n=-N}^{N} a_n(r)e^{jn\theta_a} \qquad (2)$$

where $r = \sqrt{x^2 + y^2}$ and $\theta = \arg(x, y)$ in polar coordinates. The steering condition (Equation 1), holds for functions expandable in the form of Equation (2) if and only if the interpolation functions $k_i(\theta)$ are the solutions of,

$$e^{jl\theta_a} = \sum_{i=1}^{M} e^{jl\theta_i} k_i(\theta_a), \qquad 0 \le l \le N .$$
$$(3)$$

Thus any directed impulse response of the input data can be obtained by using Equations (1-3).

Image Processing using Steerable Filters

In steerable filtering, enhancement is achieved for any arbitrary direction of the input data, while minimising the other effects in other directions. Thus steerable filters are used in various areas such as pattern recognition and fault analysis. There are many $h(x, y)$ functions, which can be chosen as steering functions satisfying Equations (1-3). Here we have chosen the two-dimensional Gaussian function as impulse response, $h(x, y) = e^{-(x^2+y^2)/2}$. As basis functions, we have derived the Gaussian function at 0 and 90 degrees as follows,

$$h^0(x, y) = \frac{\partial}{\partial x} e^{-(x^2+y^2)/2} = -2xe^{-(x^2+y^2)/2}$$
$$(4)$$
$$h^{90}(x, y) = \frac{\partial}{\partial y} e^{-(x^2+y^2)/2} = -2ye^{-(x^2+y^2)/2}$$
$$(5)$$

We can easily express impulse response of any angle of $h^\theta(x, y)$ by using basis functions given in Equation (4-5), as follows;

$$h^\theta(x, y) = \cos(\theta) \cdot h^0(x, y) + \sin(\theta) \cdot h^{90}(x, y) .$$
$$(6)$$

Thus any directed impulse response of any input image can be found by Equation 6, as a linear combination of basis functions (4) and (5). In Figure 2, the input-output relations of synthetic examples are given for $\theta = 30^0, 135^0$ degrees using Equations (7-8).

$$h^{30}(x, y) = \cos(30) \cdot h^0(x, y) +$$
$$+ \sin(30) \cdot h^{90}(x, y) = \frac{\sqrt{3}}{2} \cdot h^0(x, y) + \qquad (7)$$
$$+ \frac{1}{2} \cdot h^{90}(x, y)$$

$$h^{135}(x, y) = \cos(135) \cdot h^0(x, y) +$$
$$+ \sin(135) \cdot h^{90}(x, y) = \qquad (8)$$
$$= -\frac{\sqrt{2}}{2} \cdot h^0(x, y) + \frac{\sqrt{2}}{2} \cdot h^{90}(x, y)$$

We can conclude that the dominant effects of the input data can be extracted in the arbitrary chosen angles using steerable filters.

Application of Steerable Filters for Synthetic Examples

In this section, we have used synthetic models consisting in two prisms having magnetic property. The magnetic anomaly of these prisms is considered as input image. In the first example, two perpendicular prisms are chosen as in Figure 3a. Our aim is to evaluate the performance of steerable filtering technique in edge and corner detecting. To compare with classical approaches, we have applied Shift and Difference filters for detection of horizontal and vertical structures using Surfer8 package program as in Figure 3b and c. We have also the detected boundaries by using the boundary analysis of Blakey and Simpson (1986) (Fig. 3d).

Here we have applied streerable filters with various angles using equation 6. The steerable filter outputs are shown in Figures 3e to 3l for the angles of 0^0, 40^0, 90^0, 120^0, 160^0 and 180^0, respectively.
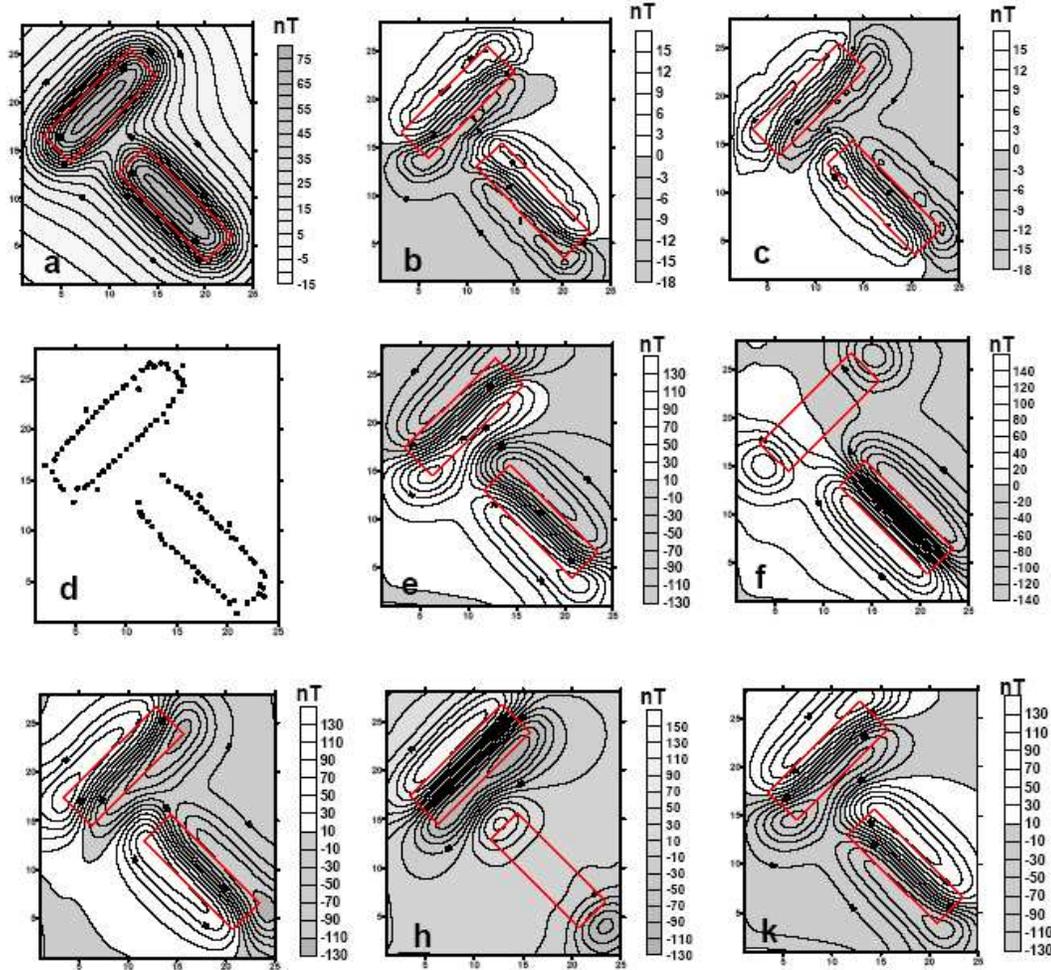
Fig 4. Two prism model having 45^0 angle in between each other (in dashed lines) with properties in Table I   **a.** Total magnetic anomaly map (interval contour is 5 nT) **b** Shift and Difference Horizontal filter output (interval contour is 3 nT) **c.** Shift and Difference Vertical filter output (interval contour is 3 nT) **d.** Boundary analysis output. **e.** Steerable filter output for the input data of total magnetic anomaly map in Figure 4a with 0^0 arbitrary angle **f.** with 45^0 **g.** with 90^0 **g.** with 135^0 **h.** with 150^0 **k.** with 180^0 (interval contour is 10 nT).

The anomalies of steerable filter output are condensed at the borders of prismatic structures. In Figure 3e, for the steering angle of 0^0, anomalies occur at in Southern and Northern regions, and they are perpendicular to each other. For 40^0, the anomalies are observed in Southern and Northern regions of these prisms as in Figure 3d to 3f. For 90^0, the anomaly coordinates are just opposite of 0^0 (Figure 3g). In the other arbitrary angles, anomalies are obtained

at the corner and borders in the direction of the angles as in Figures 3h-3l. In Figure 3l, the 180^0 steerable filter output seems similar to 0^0.

To evaluate corner detection performance of steerable filters for two prisms horizontally placed, which are perpendicular to each other. They are striking at 45^0 and 315^0 with respect to magnetic north. We have applied Shift and Difference filtering for vertical and

horizontal border detection as in Figure 4b and 3c. In Figure 4d, boundary analysis output is given. We have obtained steerable filter outputs for 0^0, 45^0, 90^0, 135^0, 150^0, 180^0, as in Figures 4e-4k, respectively. The performance of streeable filters with various angles is evaluated using the total magnetic anomaly map in Figure 4a. In Figure 4f, for 45°, anomalies are condensed on Southern and Northern regions. Thus, in this Section, we show the performance of steerable filters for vertically and horizontally placed prisms with different steering angles. In both synthetic examples, we can conclude that steerable filters are successful as in boundary analysis.

Application of Steerable Filters for Real Data: Gelibolu Region of Turkey

As an application to real data, we study on Gelibolu region of Turkey and interpret tectonic lineaments using steerable filters for the gravity and magnetic data collected by TPAO. Cramplin and Evans 1986, Barka and Kadinsky-Cade 1988, have defined tectonic regime of the area as having fault branches showing earthquake activity. Start from the Marmara Sea and pass to North-East of Aegean Sea. Yaltırak et al., (1998) have assessed the geological and tectonic structure of Gelibolu peninsula by their study in Saros Bay. Elmas and Meric (1998) have studied on the evaluation of tectonic of Marmara Sea and have given information for Gelibolu peninsula. Right lateral strike-slip fault, which defines Southern margin of the Saros Graben and Anafartalar fault, developed as positive flower structure in the late Miocene-Early Pliocene period.

In Gelibolu peninsula, there is cumulative sequence which is related to earlier ages, as it starts from West to East of the region. The oldest part of the sequence is upper cretaceous which is Lower Palaeocene aged Lort formation (Onal 1986). On this sequence, there is Karaagac formation. At the upper layer, there is Fıcıtepe formation (Kellog 1972, Yaltırak 1995). There are also

Ceylan, Mezardere, Osmancık formations on Sogucak formation and top on them Gazhanedere formation takes place (Yaltırak 1995). Gazhanedere formation continues through out the Anafartalar thrust fault (Fig. 5) is clearly observed in conventional seismic reflection data (Fig. 6).

There is an important fault in this region, named as Anafartalar at striking NE-SW as shown in Figure 5. Anafartalar inverse fault is clearly observed in the seismic section DG-158 and DG-159 (Fig. 6). Ganos fault, which is the North part of North Anatolian Fault, is located at the North-West of Gelibolu peninsula.   It is clear that Gelibolu peninsula has a complex geological structure and intense tectonics.

The vertical magnetic anomaly map of Gelibolu region obtained by TPAO is given in Figure 7a. The tectonic results are shown in Figures 7b to f, and 8b to f (Yaltırak 1998). Here we have observed prism like structures. In Figures 7b to f steerable filter outputs are given for different angles. The gravity anomaly map of the same region is as in Figure 8a. In Figure 8a, the amplitude of the gravity anomaly map increases from South-East to North-West. The increase starts at -6 mgal up to +40 mgal. We believe that one of the main reasons of this increment in amplitude is Ganos fault. The effect of Anafartalar fault and Ganos fault overlap each other, thus resulting amplitude increment and continues up to Saros Bay which lies on the West side of Gelibolu region (Ucan et al., 2001b). In Figure 8a, contour form of gravity anomaly map is drawn and in Figure 8b, clearer form is obtained.   Steerable filter outputs of gravity anomaly maps are shown in Figure 8b to f.

Here, we have applied steerable filter with various angles for the magnetic data of Gelibolu peninsula in Figure 7a, using Equations 4-6.   The steerable filtering outputs for (0^0, 40^0, 90^0, 140^0, 160^0) angles are shown in Figure 7b-7f, respectively. At 140^0 angle of filter output in Figure 7e, we observe that Anafartalar thrust fault is on the North-East direction. Especially on the
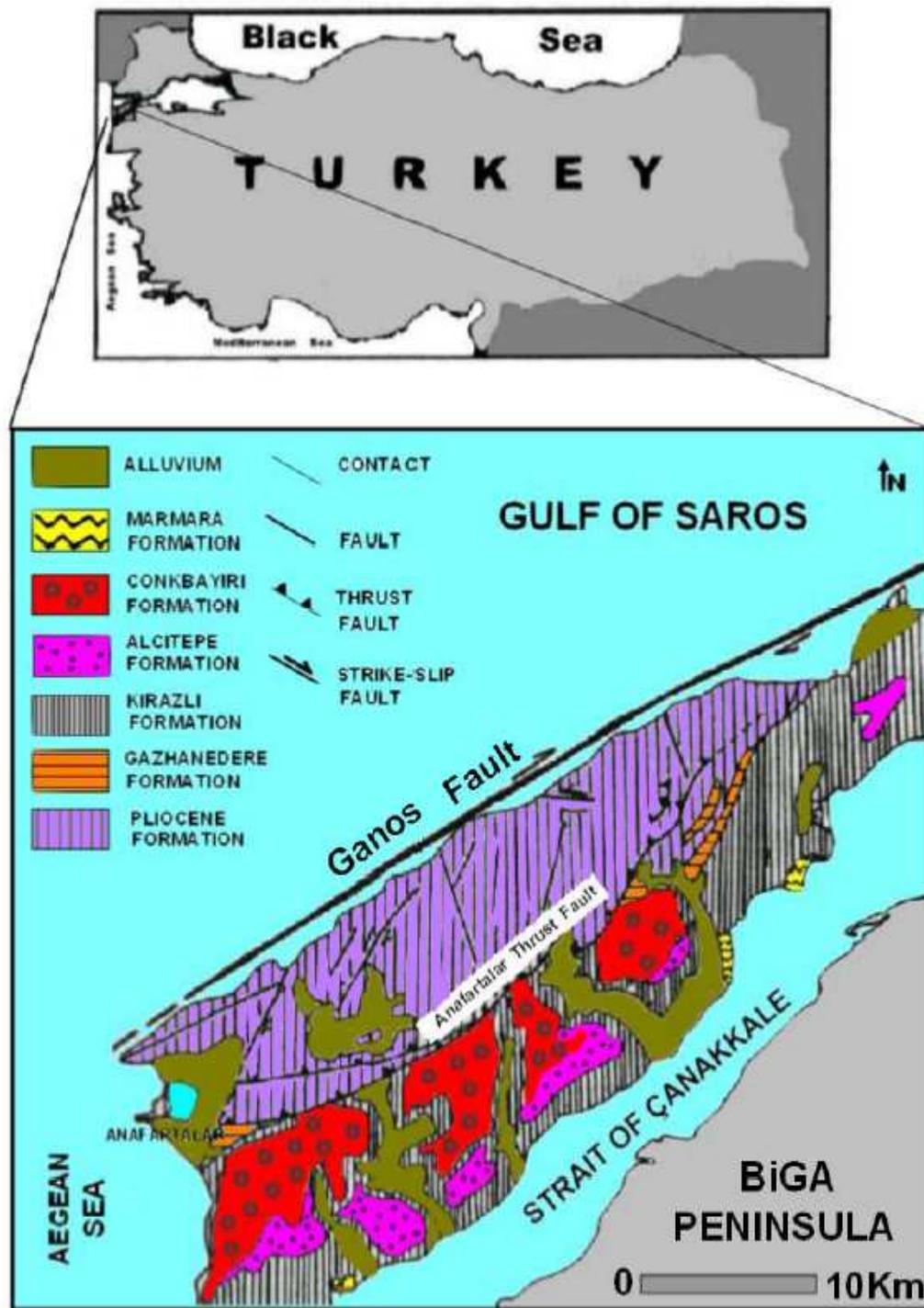
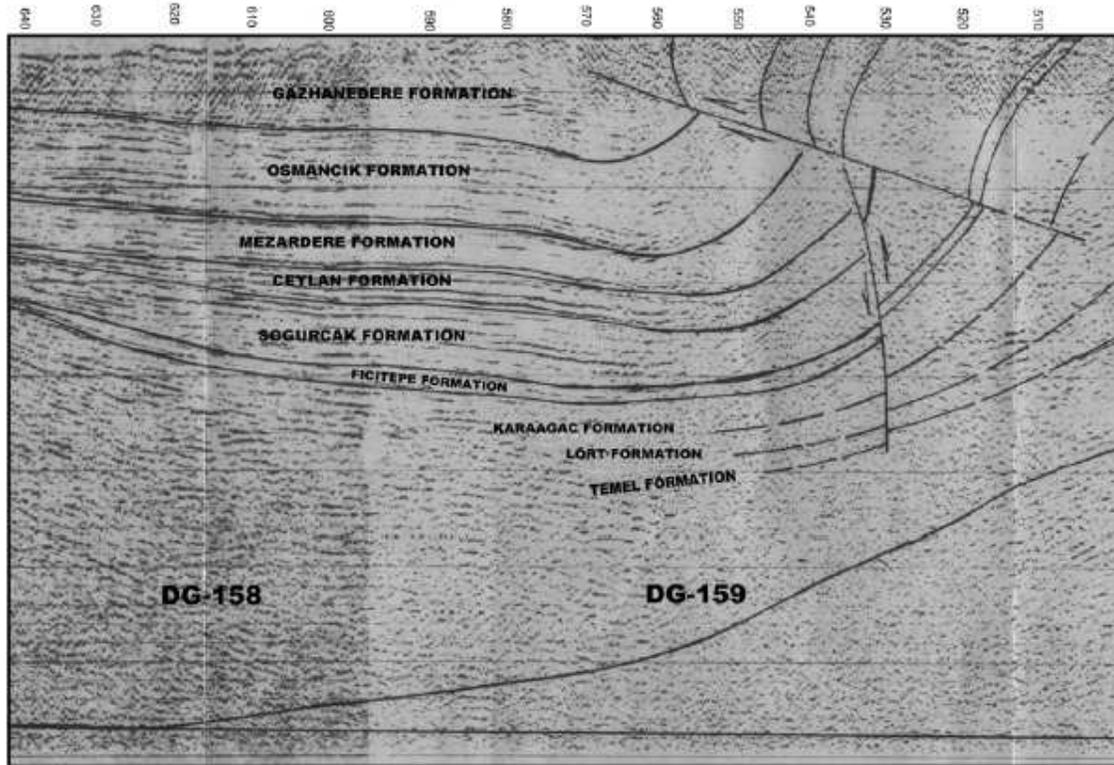**Fig 5.** Geology of Gelibolu Peninsula (modified form of Yaltirak 1995 and Yaltırak et. al 1998).

Fig 6. Deep seismic cross-sections, DG-158 and DG-159 (obtained by TPAO).

North-East direction, Anafartalar fault effect is dominant. In general overview, we conclude that Anafartalar fault has prism like structures in this region.

The contour form of Gelibolu peninsula anomaly map Figure 8a respectively. The steerable filtering outputs for (0^0, 45^0, 90^0, 120^0, 140^0) angles are shown in Figure 8b-8f, respectively. Similar results are obtained as in Figures 7 and 8. In these figures, the dominant effect of Anafartalar thrust fault is observed. We have also found out a new branch of fault at the NW of the Anafartalar thrust fault using steerable filters.

Conclusion

Steerable filters can be considered as band-pass filters with sub-band property due to the selection of arbitrary angles. In geophysics, the fault borders and their directions can be extracted by using various steerable filtering techniques, which are used in image processing, pattern recognition and other applications in electronics. The steerable filters can also be used in the detection of archeo-geophysical data and the borders of the walls and other geometric structures without distorting the ruins of historical cities.

In this paper, we have applied steerable filters in both synthetic real geophysical data. These the potential fields data used were obtained from TPAO. We have especially chosen the Gelibolu area, because it has complex structures with many faults crossing each other. We succeed to detect the borders of various synthetic examples and evaluated the fault characteristics from the real data. Especially the effect of the inverse fault is dominant. Ganos lateral fault lies on the North-West of Anafartalar and is important for its potential earthquake. In the studies of Yaltırak et al., (1995, 1998), Anafartalar fault is defined as one fault, which can be seen from geological
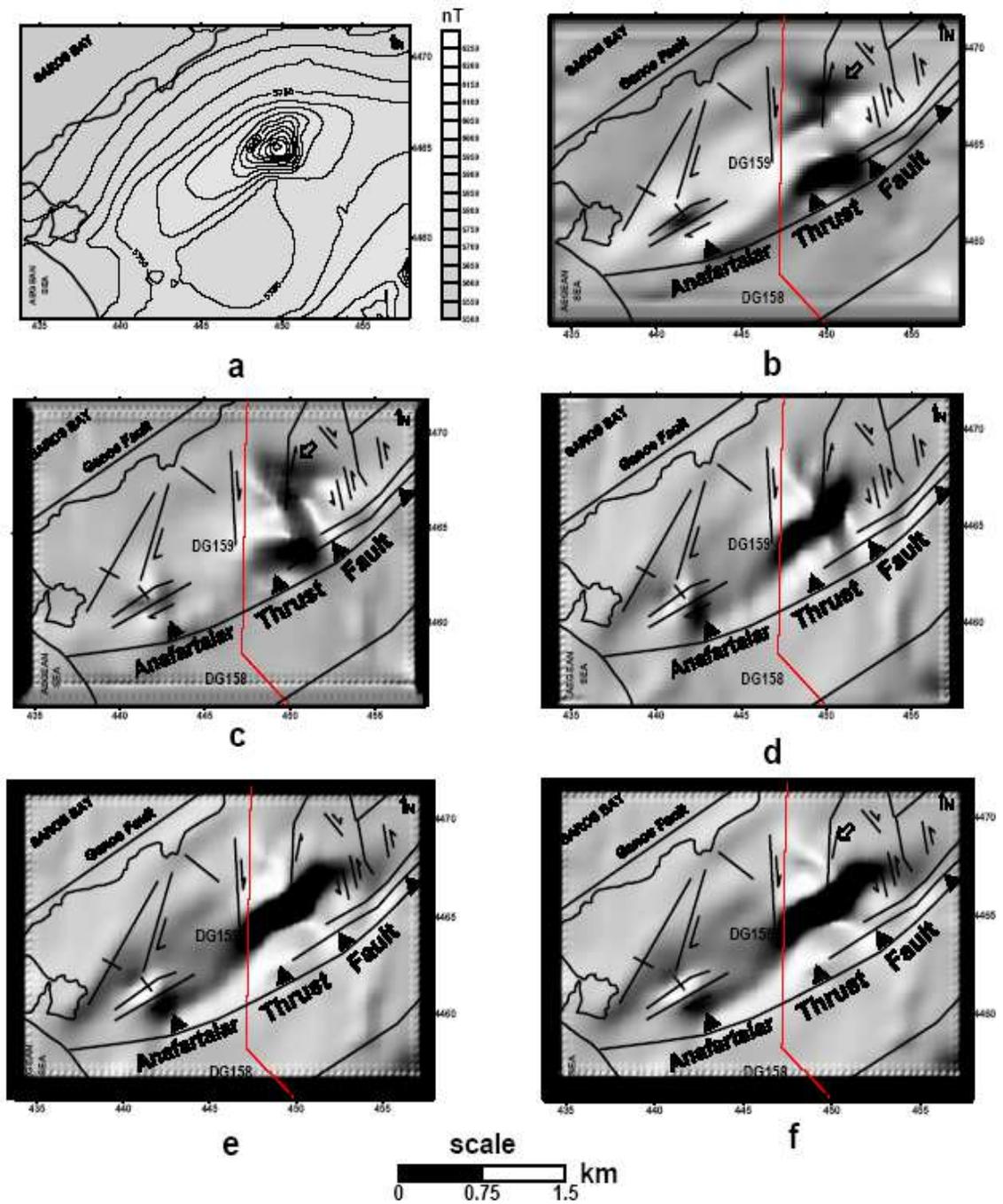
Fig. 7. Magnetic anomaly map of Gelibolu Peninsula **a.** in contoured form
(contour interval 50 nT) **b** Steerable filter output of the magnetic anomaly map obtained in
Figure 7a for angle 0^0 **c.** for 40^0 **d.** for 90^0 **e.** for 140^0 **f.** for 160^0.
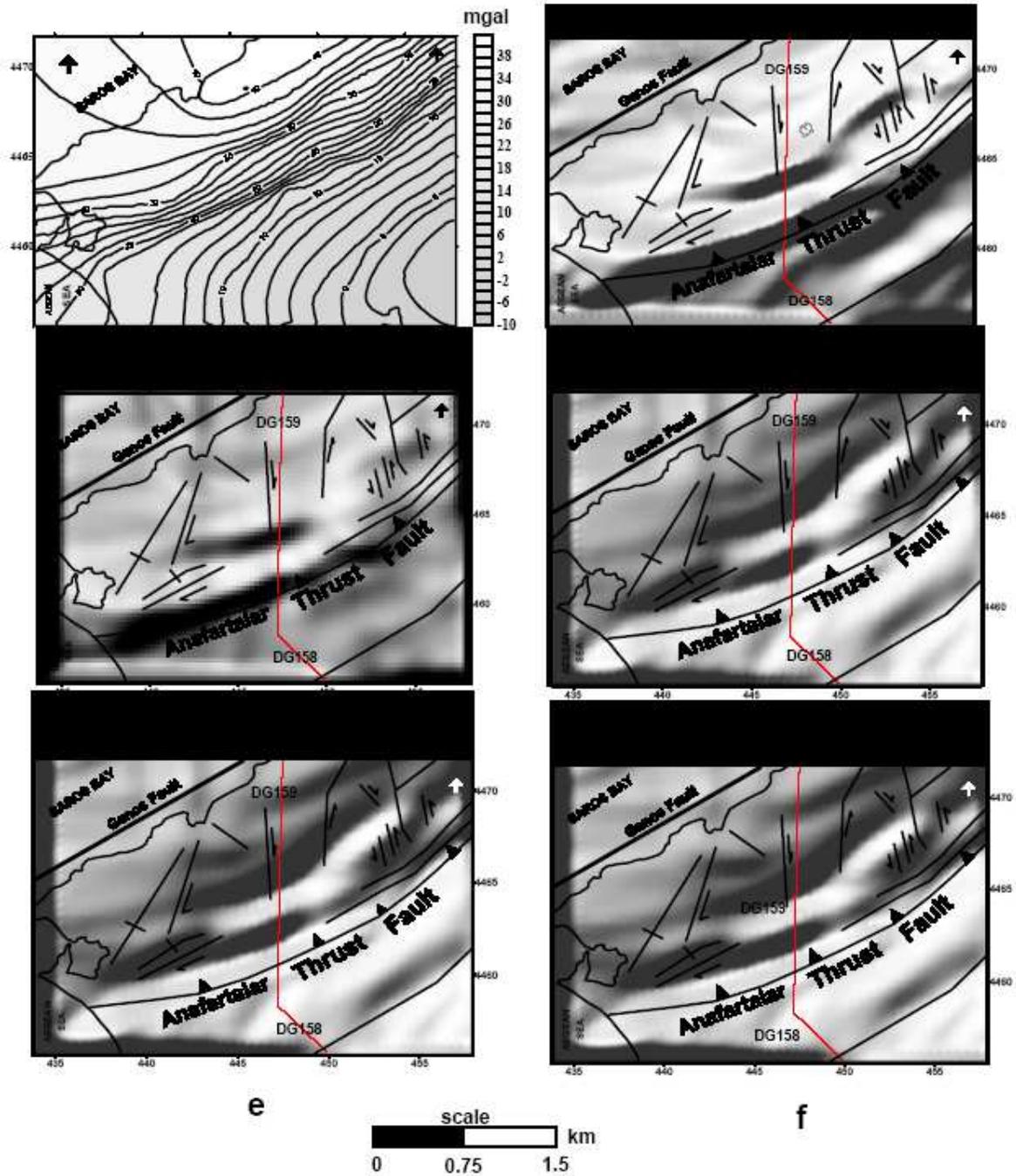
Fig. 8. Gravity anomaly map of Gelibolu Peninsula **a.** with contour form (contour interval 2 mgal) **b.** Steerable filter output of the gravity anomaly map obtained in Figure 8a for angle 0^0 **c.** for 45^0 **d.** for 120^0 **e.** for 120^0 **f.** for 140^0.
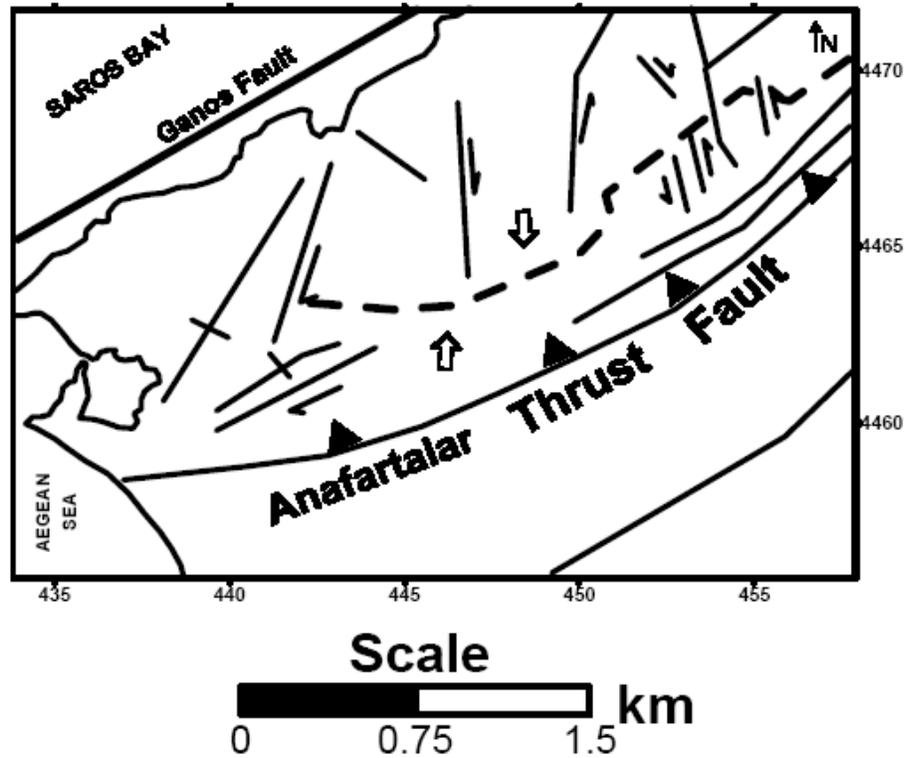
Fig. 9. Fault map obtained by the outputs of steerable filter of gravity and magnetic anomaly maps (dashed lines are proposed faults).

Table I. Magnetic anomaly map of two perpendicular prisms.

Prism	XI	X2	Y1	Y2	h	H	I	D	β	K
Num.	Coor.	Coor.	Coor.	Coor.	Top of Depth	Bottom of Depth.	Inc.	Dec.	Prism Strike	Susc.
1	15	35	33	40	1	2	60	10	0	0.001
2	39	46	4	24	1	2	60	10	0	0.001

maps. Here, we have detected another parallel fault on the North-West of Anafartalar fault using steerable filtering techniques. These results are also supported by the study of Elmas and Meriç (1998). This property is also confirmed in seismic results shown as in Figure 6. This overlapping can be explained as Anafartalar fault goes deeper and older aged faults comes up closer to the surface, resulting an active fault structure. Especially at 0^0 steerable filter output, the prismatic structure with borders and corners are well shown in Figure 7b. In steerable filtering of gravity anomaly maps, the similar structure is also observed at the NW of Anafartalar fault as in Figures 8b-8f and shown with arrows.

We have drawn the results of Yaltırak et al., (1998) in our steerable filtering of gravity and magnetic anomalies for comparison. In geological map (Figure 5), our results are confirmed by previous geological studies for the South-East of Anafartalar inverse fault, but on the North-West of this fault, we have detected another parallel fault. This finding is supported by the seismic studies done by TPAO. At DG-159 point, we study on a seismic cross-sectional data, which is perpendicular to the seismic DG-158. Anafartalar inverse fault cross section. In DG-159 cross-section, Anafartalar fault goes deeper while the structure on North-West overlaps. We can say that this overlapping is occurred due to the Ganos fault on the North and has an important tectonic effect on this region (Ucan et al., 2001b).

By considering, the new findings, we have redrawn fault map as in Figure 9. We conclude that in Gelibolu region, besides Anafartalar fault, there is also another parallel fault North-West of the later. We have shown the new fault by dashed lines. We have also used arrows to show the overlapping structure in this region.

References

Albora, A. M., Ucan, O. N., Ozmen, A., and Tulay, O., 2001a, Evaluation of Sivas-Divrigi Region Akdag Iron Ore Deposits Using Cellular Neural Network. Journal of Applied Geophysics, 46, 129-142.

Albora, A. M., Ucan, O. N., and Ozmen, A., 2001b, Residual Separation of Magnetic Fields Using a Cellular Neural Network Approach. Pure and Applied Geophysics, 158, 1797-1818.

Barka, A. A., and Kadinsky-Cade, K., 1988. Strike-slip fault geometry in Turkey and its influence on earthquake activity. Tectonics, 7, 3, 663-684.

Bilgili, E., Ucan, O. N., Albora, A. M., and Goknar, I. C., 2002. Potential Anomaly Separation Using Genetically Trained Multi-Level Cellular Neural Networks. 6th World Multiconference on systemic cybernetics and Informatics (SCI-2002), July 14-18 Florida-USA.

Blakely R.J., and Simpson R.W. 1986. Approximating edges of source bodies from aero-magnetic or gravity anomalies. Geophysics 51, 1494-1498.

Chua, L. O., and Yang, L., 1988. Cellular Neural Networks: Theory. IEEE Trans. on Circuits and Systems, 35, 1257-1272.

Chua L.O., and Thiran P., 1991, An Analytic Method For Designing Simple Cellular Neural Networks. IEEE Transactions on Circuits and Systems, Nov 1991, 38 (11): 1332-1341.

Cramplin, S., and Evans, R., 1986, Neotectonic of the Marmara Sea region in Turkey, Jour. Geol. Soc. Lond. 143, 343-348.

Derin, H., and Elliot, A. H., 1987, Modelling ans segmentation of noisy and textured images using Gibbs Random Field. IEEE PAMI, 9, 39-55.

Elmas, A., and Meric, E., 1998, The Seaway Connection between the Sea of Marmara and the Mediterranean: Tectonic Development of the Dardanelles, International Geology Review, 40, 144-162.

Fedi, M., Quata, T., 1998. Wavelet Analysis for the regional-residual and local separation at potential field anomalies. Geophysical Prospecting, 46, 507-525.

Fedi, M., and Flori, G., 2001. Detection of potential fields source boundaries by enhanced horizontal derivative method. Geophysical Prospecting, 49, 40-58.

Freeman, W. T., and Adelson, E. H. 1991. The design and use of steerable filters. IEEE Transaction on Patt. And Machine Intell., 13. 891-906.

Geman, S., and Geman, D., 1984, Stochastic Relaxation, Gibbs Distributions, and the Bayesian restration of images. IEEE PAMI, 6, 721-741

Kellog, B. H., 1972. Geology and Petroleum Prospects Gulp of Saros and vicinity

SW Trace: Ashland Oil of Turkey, TPAO Rapor No: 902.

Laine, A. F., and Chang, C. M., 1995. De-noising via wavelet transforms using steerable filters, Proc. IEEE Int. Sym. On Circuits and Systems, 3, 1956-1959.

Onal, M., 1986. Sedimentary sequences and Tectonics of central part of Gelibolu Penisula, Nortwest Anatolia, Turkey. I.U. Engineering Faculty's Earth Sciences Review, 5, 21-38.

Ozmen, A., 2001. Cellular Neural Network and Image Processing Applied. I.U. Institute of Science Technology, PhD Thesis.

Rao, R.M., Bopardikar, A.S., 1998. Wavelet Transforms Introduction to Theory and Applications. Addison Wesley Longman, USA.

Ucan, O. N., and Albora, A. M., 2001a. Evaluation of Akdag Iron Ore Reserves Using Differential Markov Random Field (DMRF), Journal of the Balkan Geoph. Soc., 3, 53-58.

Ucan O. N., Albora A. M. and Hisarli, Z. M., 2001b. Comments On The Gravity and Magnetic Anomalies of Saros Bay Using Wavelet Approach. Marine Geophysical Researches, **22,** 251-264.

Yaltırak, C., 1995. Tectonic Mechanism Controlling the Plio-Quaternary Sedimentation in the Gelibolu Peninsula. Turkish Gephsics (Nezihi Canitez Semposium). 9, 103-106.

Yaltırak, C., Alpar, B. and Yuce, H., 1998. Tectonic elements controlling the evolution of the Gulf of Saros (norteastern Aegean Sea, Turkey). Tectonophysics, 300, 227-248.

Zou, F., and Nossek, J. A., 1991. Stability Of Cellular Neural Networks with Opposite-Sign Templates. IEEE Transactions On Circuits And Systems, Jun 1991, 38 (6): 675 – 677.